crystals

MDPI

Article

Synthesis, X-ray, Hirshfeld, and AIM Studies on Zn(II) and Cd(II) Complexes with Pyridine Ligands

Mezna Saleh Altowyan [1], Eman M. Fathalla [2], Dalia Hawas [2], Jörg H. Albering [3], Assem Barakat [4], Morsy A. M. Abu-Youssef [2,*], Saied M. Soliman [2,*], Taher S. Kassem [2] and Ahmed M. A. Badr [2]

1 Department of Chemistry, College of Science, Princess Nourah bint Abdulrahman University, P.O. Box 84428, Riyadh 11671, Saudi Arabia; msaltowyan@pnu.edu.sa
2 Department of Chemistry, Faculty of Science, Alexandria University, P.O. Box 426, Ibrahimia, Alexandria 21321, Egypt; Eman.nomeir@alexu.edu.eg (E.M.F.); daliah_207@hotmail.com (D.H.); taher.kassem.2011@gmail.com (T.S.K.); ahmed_badr@alexu.edu.eg (A.M.A.B.)
3 Graz University of Technology, Mandellstr. 11/III, A-8010 Graz, Austria; joerg.albering@tugraz.at
4 Department of Chemistry, College of Science, King Saud University, P.O. Box 2455, Riyadh 11451, Saudi Arabia; ambarakat@ksu.edu.sa
* Correspondence: Morsy5@AlexU.edu.eg (M.A.M.A.-Y.); saied1soliman@yahoo.com or saeed.soliman@alexu.edu.eg (S.M.S.)

Abstract: The synthesis and crystal structures of three heteroleptic complexes of Zn(II) and Cd(II) with pyridine ligands (ethyl nicotinate (**EtNic**), N,N-diethylnicotinamide (**DiEtNA**), and 2-amino-5-picoline (**2Ampic**) are presented. The complex **[Zn(EtNic)$_2$Cl$_2$]** (**1**) showed a distorted tetrahedral coordination geometry with two **EtNic** ligand units and two chloride ions as monodentate ligands. Complexes **[Zn(DiEtNA)(H$_2$O)$_4$(SO$_4$)]·H$_2$O** (**2**) and **[Cd(OAc)$_2$(2Ampic)$_2$]** (**3**) had hexa-coordinated Zn(II) and Cd(II) centers. In the former, the Zn(II) was coordinated with three different monodentate ligands, which were **DiEtNA**, H_2O, and SO_4^{2-}. In **3**, the Cd(II) ion was coordinated with two bidentate acetate ions and two monodentate **2Ampic** ligand units. The supramolecular structures of the three complexes were elucidated using Hirshfeld analysis. In **1**, the most important interactions that governed the molecular packing were O···H (15.5–15.6%), Cl···H (13.6–13.8%), Cl···C (6.3%), and C···H (10.3–10.6%) contacts. For complexes **2** and **3**, the H···H, O···H, and C···H contacts dominated. Their percentages were 50.2%, 41.2%, and 7.1%, respectively, for **2** and 57.1%, 19.6%, and 15.2%, respectively, for **3**. Only in complex **3**, weak π-π stacking interactions between the stacked pyridines were found. The Zn(II) natural charges were calculated using the DFT method to be 0.8775, 1.0559, and 1.2193 for complexes **1**–**3**, respectively. A predominant closed-shell character for the Zn–Cl, Zn–N, Zn–O, Cd–O, and Cd–N bonds was also concluded from an atoms in molecules (AIM) study.

Keywords: cadmium(II); zinc(II); pyridine-type ligand; Hirshfeld; intermolecular interactions; X-ray

check for updates

Citation: Altowyan, M.S.; Fathalla, E.M.; Hawas, D.; Albering, J.H.; Barakat, A.; Abu-Youssef, M.A.M.; Soliman, S.M.; Kassem, T.S.; Badr, A.M.A. Synthesis, X-ray, Hirshfeld, and AIM Studies on Zn(II) and Cd(II) Complexes with Pyridine Ligands. *Crystals* **2022**, *12*, 590. https://doi.org/10.3390/cryst12050590

Academic Editor: Ulli Englert

Received: 29 March 2022
Accepted: 20 April 2022
Published: 22 April 2022

Publisher's Note: MDPI stays neutral with regard to jurisdictional claims in published maps and institutional affiliations.

1. Introduction

Metallosupramolecular complexes are currently attracting a lot of attention because of their diverse uses in different applications, such as gas storage, optics, catalysis, electronic conductivity, and magnetism [1–25]. Non-covalent interactions, namely aromatic π···π stacking and H-bonding interactions, are important for the construction of supramolecular structures from the self-assembly of diverse components [26–32]. These interactions, along with van der Waals forces, play important roles in a variety of domains, including crystal engineering, inorganic chemistry, biochemistry, and others [33–36].

Different metal ions have various characteristics and different modes of coordination, which represent important factors in determining the molecular and supramolecular structures of complexes. For instance, metal ions with d^{10} configurations, such as Zn(II) and Cd(II), when reacting with organic ligands, frequently exhibit several coordination numbers [37–40]. With their spherical d^{10} configuration, these metal ions show rather spherical

and non-selective coordination, with coordination numbers simply governed by the size of the metal ion and the ligands. Because of their structural flexibility and their significance as luminescent materials and in ligand exchange chromatography, this category of complexes has received a lot of attention [41–45]. In addition, complexes of Zn(II) have interesting biological applications [46]. Among neutral aromatic N-donor ligands, pyridine derivatives are important ligands [47] for constructing various coordination compounds [48–53] with diverse applications [54–56]. These compounds can be used to treat brain illnesses and neurological diseases and are also used as an anesthetic, anti-inflammatory, and anti-cancer agent [57]. Additionally, the nature of the small anion has a significant impact on the complex's structure [58–63]. Hence, combining metal ions with nitrogen donor ligands and a small anionic oxygen donor could be a way to synthesize new heteroleptic complexes.

In this work, new Zn(II) and Cd(II) complexes with the pyridine derivatives (Figure 1) ethyl nicotinate (**EtNic**), N,N-diethylnicotinamide (**DiEtNA**), and 2-amino-5-picoline (**2Ampic**) were synthesized, and their supramolecular structures were characterized using X-ray single-crystal structure and Hirshfeld analyses. The charge distribution and bonding were studied using DFT-based natural charge calculations and the atoms in molecules (AIM) method.

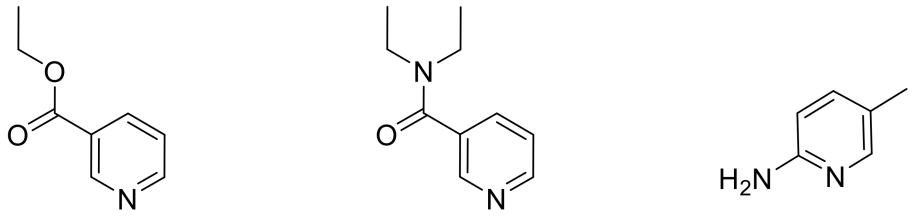

EtNic **DiEtNA** **2Ampic**

Figure 1. Structures of the studied ligands **EtNic** [64–66], **DiEtNA** [67–70] and **2Ampic** [71–73].

2. Materials and Methods

2.1. Materials and Physical Measurements

All chemicals and reagents used were of analytical grade and were used without additional purification, as received from Sigma-Aldrich Chemical Company Inc. (St. Louis, MO, USA). CHN analysis was performed using a PerkinElmer 2400 Elemental Analyzer (PerkinElmer Inc., Waltham, MA, USA). The metal content was measured with a Shimadzu atomic absorption spectrophotometer (AA-7000 series, Shimadzu, Ltd., Kyoto, Japan).

2.2. Synthesis of Complexes **1**–**3**

A similar procedure was used to prepare the three complexes. An aqueous solution of the metal salt was mixed with an ethanolic solution of the functional ligand. The resulting clear solution was left for slow evaporation at room temperature for a couple of days. After a week, colorless crystals of the target compounds suitable for X-ray analysis were obtained.

2.2.1. **[Zn(EtNic)$_2$Cl$_2$]** (**1**)

Complex **1** was prepared by mixing a 10 mL aqueous solution of $ZnCl_2$ (13.6 mg, 0.1 mmol) with a 10 mL ethanolic solution of **EtNic** (30.2 mg, 0.2 mmol). $C_{16}H_{18}Cl_2N_2O_4Zn$: Yield: 85%; Anal. Calc.: C, 43.81; H, 4.14; N, 6.39; Zn, 14.91%. Found: C, 43.50; H, 4.06; N, 6.25; Zn, 14.79%.

2.2.2. **[Zn(DiEtNA)(H$_2$O)$_4$(SO$_4$)]·H$_2$O** (**2**)

Complex **2** was prepared by mixing equimolar amounts of a 10 mL aqueous solution of $ZnSO_4.7H_2O$ (28.8 mg, 0.1 mmol) with a 10 mL ethanolic solution of **DiEtNA** (17.8 mg, 0.1 mmol). $C_{10}H_{24}N_2O_{10}SZn$: Yield: 79%; Anal. Calc.: C, 27.95; H, 5.63; N, 6.52; Zn, 15.22%. Found: C, 27.74; H, 5.54; N, 6.39; Zn, 15.05%.

2.2.3. **[Cd(OAc)$_2$(2Ampic)$_2$]** (**3**)

Complex **3** was prepared by mixing a 10 mL aqueous solution of Cd(OAc)$_2$ (23.0 mg, 0.1 mmol) with a 10 mL ethanolic solution of **2Ampic** (21.6 mg, 0.2 mmol). $C_{16}H_{22}Cd\,N_4O_4$: Yield: 81%; Anal. Calc.: C, 43.01; H, 4.96; Cd, 25.16; N, 12.54%. Found: C, 42.72; H, 4.85; Cd, 25.06; N, 12.33%

2.3. Crystal Structure Determination

The crystal structure determinations for complexes **1**–**3** are described in method S1 and Table S1 (Supporting Materials) [74,75].

2.4. Hirshfeld Surface Analysis

The Crystal Explorer Ver. 3.1 [76] program was used to construct the Hirshfeld surfaces and determine the 2D fingerprint plot for the studied complexes [77,78].

2.5. DFT Calculations

All DFT computations were performed using Gaussian 09 software [79]. Natural charge calculations [80] were performed at the MPW1PW91 [81] level combined with cc-PVTZ and cc-PVTZ-PP basis sets for nonmetal and metal atoms, respectively [82,83]. Atoms in molecules (AIM) parameters were calculated [84] using the Multiwfn program [85].

3. Results and Discussion

3.1. X-ray Structure Description

3.1.1. Structure of **[Zn(EtNic)$_2$Cl$_2$]**; **1**

The X-ray structure of the heteroleptic Zn(II) complex **1** is shown in Figure 2. The complex crystallized in the monoclinic crystal system and $P2_1/c$ space group. The unit cell parameters were a = 14.1940(9) Å, b = 19.8380(11) Å, c = 14.3957(9), Å and β = 111.432(3)°. The view of the unit cell of **1** along the *ac* plane is shown in Figure S1 (Supporting Materials). The asymmetric unit comprised two **[Zn(EtNic)$_2$Cl$_2$]** formula units. The Zn(II) was coordinated with two **EtNic** molecules via the ring N-atom and two chloride ions. The Zn–N distances were marginally different (2.057(3)–2.061(3) Å), and the same is true for the Zn–Cl bonds (2.221(1)–2.226(1) Å). The N-Zn-N and Cl-Zn-Cl angles were in the ranges of 110.68(13)–110.84(13)° and 129.13(4)–129.46(4)°, respectively (Table 1). Hence, Zn(II) was tetra-coordinated with a distorted tetrahedral coordination environment, which is expected for a small size metal ion with a spherical d^{10} configuration.

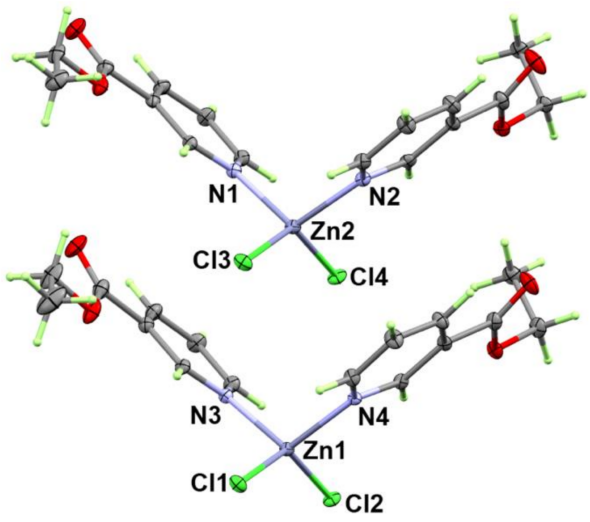

Figure 2. The asymmetric unit of the **[Zn(EtNic)$_2$Cl$_2$]** complex.

Table 1. The important geometric parameters (Å, °) in complex **1**.

Bond	Distance	Bond	Distance
Zn1-N4	2.057(3)	Zn2-N2	2.059(3)
Zn1-N3	2.057(3)	Zn2-N1	2.061(3)
Zn1-Cl1	2.222(1)	Zn2-Cl3	2.2221(1)
Zn1-Cl2	2.224(1)	Zn2-Cl4	2.226(1)
Bonds	Angle	Bonds	Angle
N4-Zn1-N3	110.84(13)	N2-Zn2-N1	110.68(13)
N4-Zn1-Cl1	103.87(8)	N2-Zn2-Cl3	104.85(8)
N3-Zn1-Cl1	104.79(9)	N1-Zn2-Cl3	105.46(9)
N4-Zn1-Cl2	103.58(8)	N2-Zn2-Cl4	102.29(9)
N3-Zn1-Cl2	103.84(8)	N1-Zn2-Cl4	103.91(8)
Cl1-Zn1-Cl2	129.46(4)	Cl3-Zn2-Cl4	129.13(4)

The supramolecular structure of **1** is controlled by weak non-classical C-H···O interactions between the protons from the CH_2 group in the ester moiety of one molecule with the oxygen atom of the carbonyl group in the ester moiety of another molecule. As can be seen from the packing scheme shown in Figure 3, the C7-H7A···O5 and C31-H31B···O4 interactions form a wave-like chain along the *a*-direction. The hydrogen bond parameters are depicted in Table S2 (Supporting Materials). The H7A···O5 and H31B···O4 distances were 2.58 and 2.55 Å, respectively. In addition, the corresponding donor–acceptor distances were 3.076(5) and 3.055(6) Å, respectively.

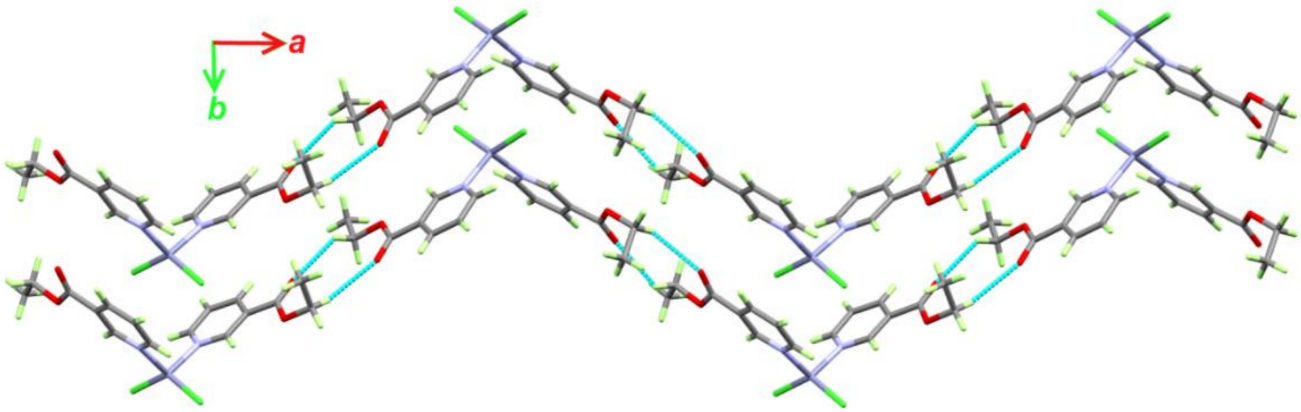

Figure 3. Wave-like packing of **1** along the a*b* plane.

3.1.2. Structure of **[Zn(DiEtNA)(H_2O)$_4$(SO_4)]·H_2O**; **2**

The X-ray structure of **2** also revealed a heteroleptic Zn(II) complex, but in this case, the Zn(II) was hexa-coordinated (Figure 4). This complex crystallized in the orthorhombic crystal system and $P2_12_12_1$ space group. The unit cell parameters were a = 7.6541(3) Å, b = 9.9244(4), Å and c = 23.1526(10) Å. The asymmetric unit comprised one **[Zn(DiEtNA)(H_2O)$_4$(SO_4)]·H_2O** formula unit. The view of the unit cell of **2** along the *ac* plane is shown in Figure S2 (Supporting Materials). In this complex, the Zn(II) was hexa-coordinated to only one bulky **DiEtNA** organic ligand; five small ligands, which were the four water molecules; and one sulfate anion, all acting as monodentate ligands. The structure of this complex comprised one crystal water, which was not a part of the coordination sphere but contributed significantly to the molecular packing of this complex. Among the five Zn-O interactions, the longest zinc-to-oxygen distance was Zn1-O9 (2.1284(10) Å), which occurred with the weakly coordinated sulfate anion. By contrast, the Zn1-O4 bond, which occurred between the Zn(II) ion and the water molecule *trans* to the Zn1-O9 bond, was the shortest (2.0657(11) Å). Additionally, the distance between the Zn(II) and the heterocyclic nitrogen of **DiEtNA** was 2.1388(12) Å. In addition, the bond angles

inside the coordination sphere deviated from the ideal values of 180 and 90° for the *trans* and *cis* bonds, respectively (Table 2). The angles between the *trans* bonds ranged from 174.37(4)° (O4-Zn1-O9) to 177.53(5)° (O3-Zn1-O2), while the angles between the *cis* bonds were in the range of 83.99(4)° (O5-Zn1-O9) to 92.91(4)° (O4-Zn1-N1). The distance between the Zn(II) ion and the oxygen of the crystal water was 4.325(3) Å, which is too long to be a bond. Hence, the fifth water molecule was a part of the outer sphere.

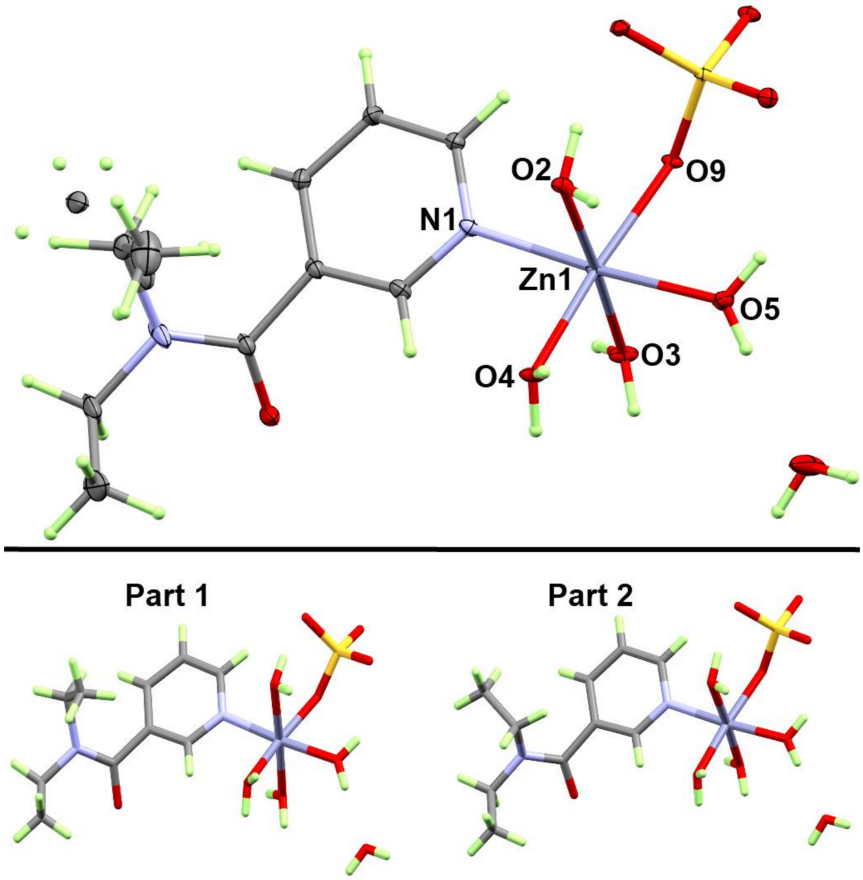

Figure 4. The asymmetric unit of **[Zn(DiEtNA)(H_2O)$_4$(SO_4)]·H_2O (2)**. The disorder of one of the ethyl groups was refined as Part 1 (59.7%) and Part 2 (40.3%).

Table 2. The important geometric parameters (Å, °) in complex **2**.

Bond	Distance	Bond	Distance
Zn1-O4	2.0657(11)	Zn1-O2	2.1146(11)
Zn1-O3	2.0796(11)	Zn1-O9	2.1284(10)
Zn1-O5	2.1012(11)	Zn1-N1	2.1388(12)
Bonds	**Angle**	**Bonds**	**Angle**
O4-Zn1-O3	92.35(4)	O5-Zn1-O9	83.99(4)
O4-Zn1-O5	90.56(5)	O2-Zn1-O9	92.84(4)
O3-Zn1-O5	92.27(5)	O4-Zn1-N1	92.91(4)
O4-Zn1-O2	85.66(4)	O3-Zn1-N1	89.26(5)
O3-Zn1-O2	177.53(5)	O5-Zn1-N1	176.15(5)
O5-Zn1-O2	89.20(5)	O2-Zn1-N1	89.39(5)
O4-Zn1-O9	174.37(4)	O9-Zn1-N1	92.50(4)
O3-Zn1-O9	89.28(4)		

In contrast to **1**, the supramolecular structure of **2** was controlled by several strong O-H···O hydrogen bonds (Table 3). The coordinated and crystal water molecules acted as

hydrogen bond donors, while the oxygen atoms from the amide group, the coordinated sulfate ion, and the crystal water were the hydrogen bond acceptors. In addition, the structure was found to be stabilized by some intramolecular O···H interactions. The intra- and intermolecular hydrogen bonds are shown in Figure 5A as turquoise and red dotted lines, respectively, while the 3D packing structure is shown in Figure 5B.

Table 3. Hydrogen bond parameters (Å, °) in **2**.

D-H···A	d(D-H)	d(H···A)	d(D···A)	<(DHA)	Symm. Code
O2-H2A···O9	0.86(2)	1.90(2)	2.7561(15)	173(2)	−x,−1/2 + y,1/2 − z
O2-H2B···O7	0.845(16)	1.996(17)	2.7789(14)	153.7(18)	
O3-H3A···O6	0.82(2)	1.93(2)	2.7429(15)	176(2)	1 + x,y,z
O3-H3B···O8	0.83(2)	2.00(2)	2.8216(15)	170(2)	−x,1/2 + y,1/2 − z
O4-H4A···O7	0.831(16)	1.829(16)	2.6591(15)	177(2)	1 + x,y,z
O4-H4B···O6	0.82(2)	1.91(2)	2.7266(14)	170(3)	−x,−1/2 + y,1/2 − z
O5-H5A···O8	0.81(2)	2.32(2)	2.9958(16)	141(2)	
O5-H5B···O10	0.77(3)	1.92(3)	2.680(2)	174(3)	
O10-H10A···O1	0.77(2)	1.97(3)	2.734(3)	178(3)	1 − x,−1/2 + y,1/2 − z
O10-H10B···O8	0.81(3)	2.09(3)	2.8874(19)	169(4)	1 + x,y,z
C1-H1···O7	0.95	2.54	3.3586(18)	144	
C2-H2···O1	0.95	2.35	3.2622(19)	160	−1 + x,y,z
C3-H3···O1	0.95	2.58	3.260(2)	129	−1/2 + x,3/2 − y,−z
C5-H5···O4	0.95	2.53	3.0950(18)	118	

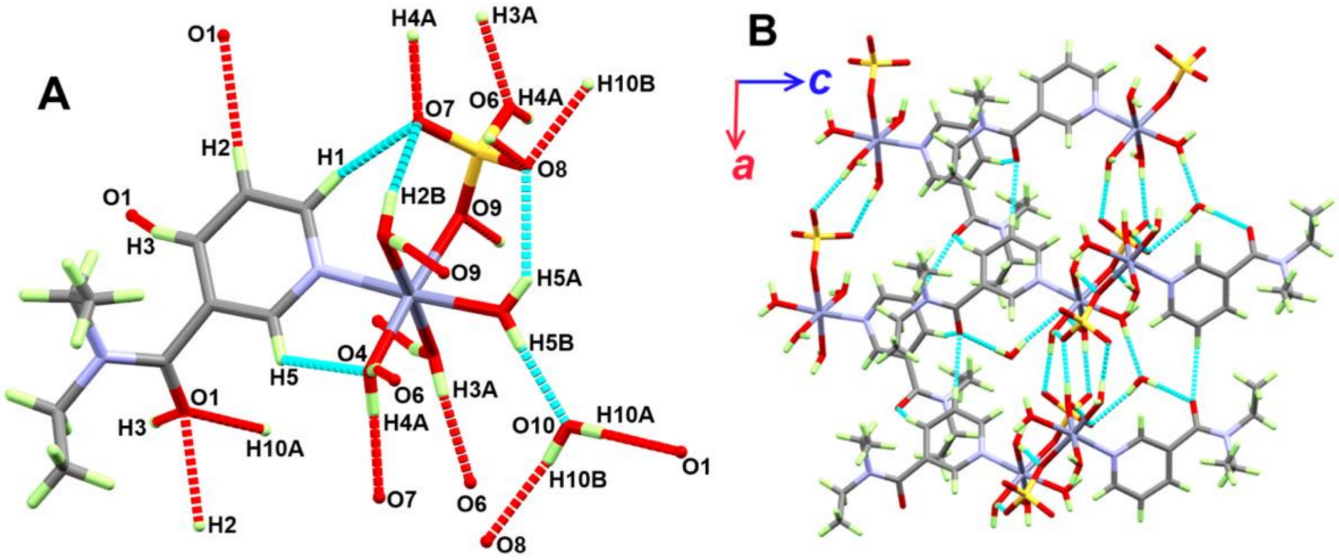

Figure 5. Intra- and intermolecular contacts (**A**) through O-H···O hydrogen bonds and packing of **2** along the *ac* plane (**B**).

3.1.3. Structure of **[Cd(OAc)$_2$(2Ampic)$_2$]**; **3**

The X-ray structure of the **[Cd(OAc)$_2$(2Ampic)$_2$]** complex **3** is shown in Figure 6. This compound crystallized in the monoclinic crystal system and $P2_1/n$ space group. The unit cell parameters were a = 8.4025(4) Å, b = 17.1565(15) Å, c = 12.9867(9) Å, and β = 94.661(3)°. The view of the unit cell of **3** along the *bc* plane is shown in Figure S3 (Supporting Materials). In this complex, the large Cd(II) ion was hexa-coordinated with the heterocyclic nitrogen atom of the two bulky **2Ampic** molecules, which acted as the monodentate ligand. In addition, the Cd(II) was coordinated with four oxygen atoms from two bidentate acetate ions. The Cd1-N1 and Cd1-N2 distances were 2.3210(8) and 2.2723(8) Å, respectively, while the N1-Cd1-N2 angle was 93.39(3)°, indicating that the two pyridine ligand units are located *cis* to one another. On the other hand, the acetate group of the lower atom numbering

had different Cd-to-O distances. The Cd1-O1 and Cd1-O2 distances were 2.2993(7) and 2.4484(7) Å, respectively. The other acetate group had two almost equidistant Cd-O bonds, for which the Cd1-O3 and Cd1-O4 distances were 2.3813(8) and 2.3356(7) Å, respectively. The bite angles of the two acetate groups were 55.08(2) and 55.67(3)°, respectively (Table 4). Because of the small bite angles of the two acetate groups, one could consider that the two acetate ions are also located *cis* to each other.

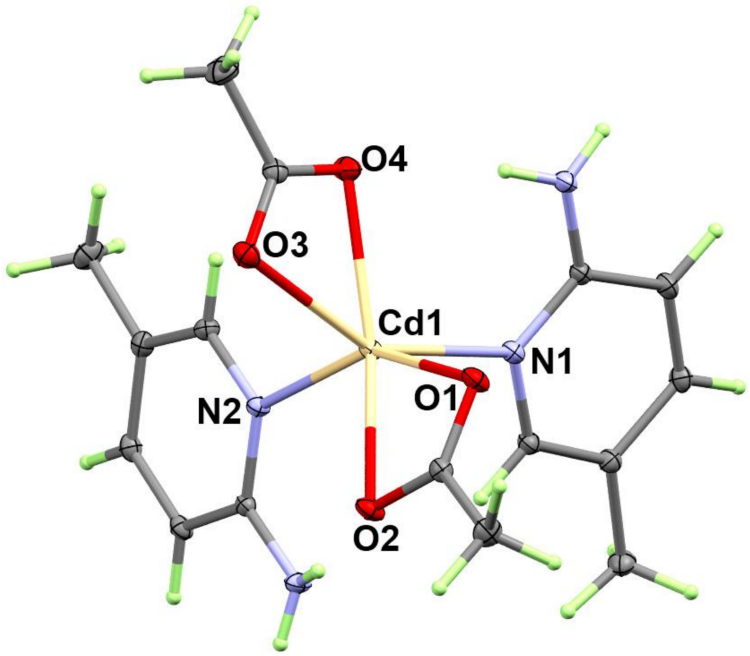

Figure 6. The asymmetric unit of **[Cd(OAc)$_2$(2Ampic)$_2$]** (**3**).

Table 4. The important geometric parameters (Å, °) in complex **3**.

Bond	Distance	Bond	Distance
Cd1-N2	2.2723(8)	Cd1-O4	2.3356(7)
Cd1-O1	2.2993(7)	Cd1-O3	2.3813(8)
Cd1-N1	2.3210(8)	Cd1-O2	2.4484(7)
Bonds	Angle	Bonds	Angle
N2-Cd1-O1	150.61(3)	N1-Cd1-O3	150.41(3)
N2-Cd1-N1	93.39(3)	O4-Cd1-O3	55.67(3)
O1-Cd1-N1	91.69(3)	N2-Cd1-O2	96.04(2)
N2-Cd1-O4	101.74(3)	O1-Cd1-O2	55.08(2)
O1-Cd1-O4	106.61(3)	N1-Cd1-O2	108.94(3)
N1-Cd1-O4	95.09(3)	O4-Cd1-O2	149.13(3)
N2-Cd1-O3	96.88(3)	O3-Cd1-O2	97.50(3)
O1-Cd1-O3	92.77(3)		

The supramolecular structure of **3** is controlled by a complicated set of classical (N-H···O) and non-classical (C-H···O) hydrogen bonding interactions (Table 5). The molecular structure of **3** is stabilized by the intramolecular N3-H3A···O4 and N4-H4D···O2 hydrogen bonds, which are shown in Figure 7A as turquoise dotted lines, while the intermolecular hydrogen bonds are shown in the same figure as red dotted lines. The 3D packing structure of complex **3** is shown along the *ab* plane in Figure 7B.

Table 5. Hydrogen bond parameters (Å, °) in **3**.

D-H···A	d(D-H)	d(H···A)	d(D···A)	<(DHA)	Symm. Code
N3-H3A···O4	0.845(16)	2.102(16)	2.9333(12)	167.6(16)	
N3-H3B···O2	0.862(15)	2.151(15)	3.0047(11)	70.9(15)	−1 + x,y,z
N4-H4D···O2	0.827(17)	2.188(17)	3.0046(11)	169.4(15)	
N4-H4E···O1	0.839(16)	2.097(16)	2.9181(12)	165.9(15)	1/2 + x,1/2 − y,1/2 + z
C7-H7···O3	0.95	2.55	3.2791(13)	134	2 − x,1 − y,2 − z
C8-H8···O1	0.95	2.56	3.3046(13)	135	1/2 + x,1/2 − y,1/2 + z
C10-H10C···O4	0.98	2.56	3.4072(14)	145	1 − x,1 − y,2 − z
C13-H13···O3	0.95	2.57	3.3091(12)	135	−1/2 + x,1/2 − y,1/2 + z

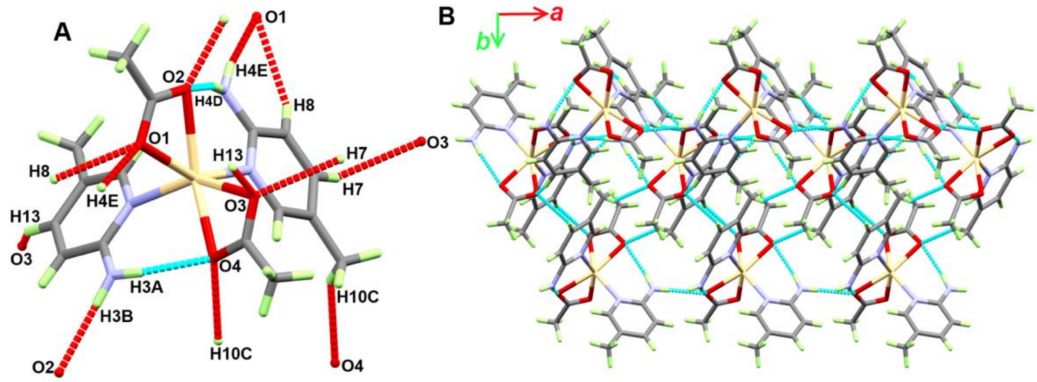

Figure 7. The intra- and intermolecular contacts (**A**) and packing scheme via O-H···O hydrogen bonds along a*b* plane (**B**) of **3**.

3.2. Hirshfeld Surface Analysis

The use of Hirshfeld surface analysis to describe the intermolecular interactions that affect the molecule packing in crystals has been shown to be very effective [86]. In this context, various contacts in the crystal structures of the investigated complexes were quantitatively evaluated using Hirshfeld calculations. For complex **1**, the single-crystal X-ray structure showed the presence of two **[Zn(EtNic)$_2$Cl$_2$]** units per asymmetric formula (**Zn1** and **Zn2** units), so there are two sets of results for this crystal structure (Table 6). It is clear that the types of interactions, as well as their percentages in both units, were nearly identical, and the most predominant contacts in both units were H···H, O···H, Cl···H, C···H, and Cl···C (Table 6). Their percentages were 43.8%, 15.6%, 13.6%, 10.6%, and 6.3%, respectively, for the **Zn1** unit and 44.0%, 15.5%, 13.8%, 10.3%, and 6.3%, respectively, for the **Zn2** unit.

Table 6. Different contacts and their percentages in complex **1**.

Contact	Zn1 Unit	Zn2 Unit
Zn···N	0.5	0.5
Zn···C	1.1	1.1
Cl···N	1.5	1.5
Cl···O	1.1	1.1
Cl···C	6.3	6.3
Cl···H	13.6	13.8
N···C	2.3	2.3
N···H	0.8	0.7
O···O	0.2	0.2
O···C	2.2	2.2
O···H	15.6	15.5
C···C	0.4	0.4
C···H	10.6	10.3
H···H	43.8	44

The decomposed d_{norm} maps and fingerprint plots strongly show that O···H, Cl···H, Cl···C, and C···H are the most important interactions that govern the molecular packing of **1**. The appearance of these contacts as red spots in the d_{norm} maps and relatively sharp spikes in the fingerprint plots (Figure 8) reveal the importance of these short contacts in the crystal stability of this complex. The contact distances of all the short contacts are listed in Table 7.

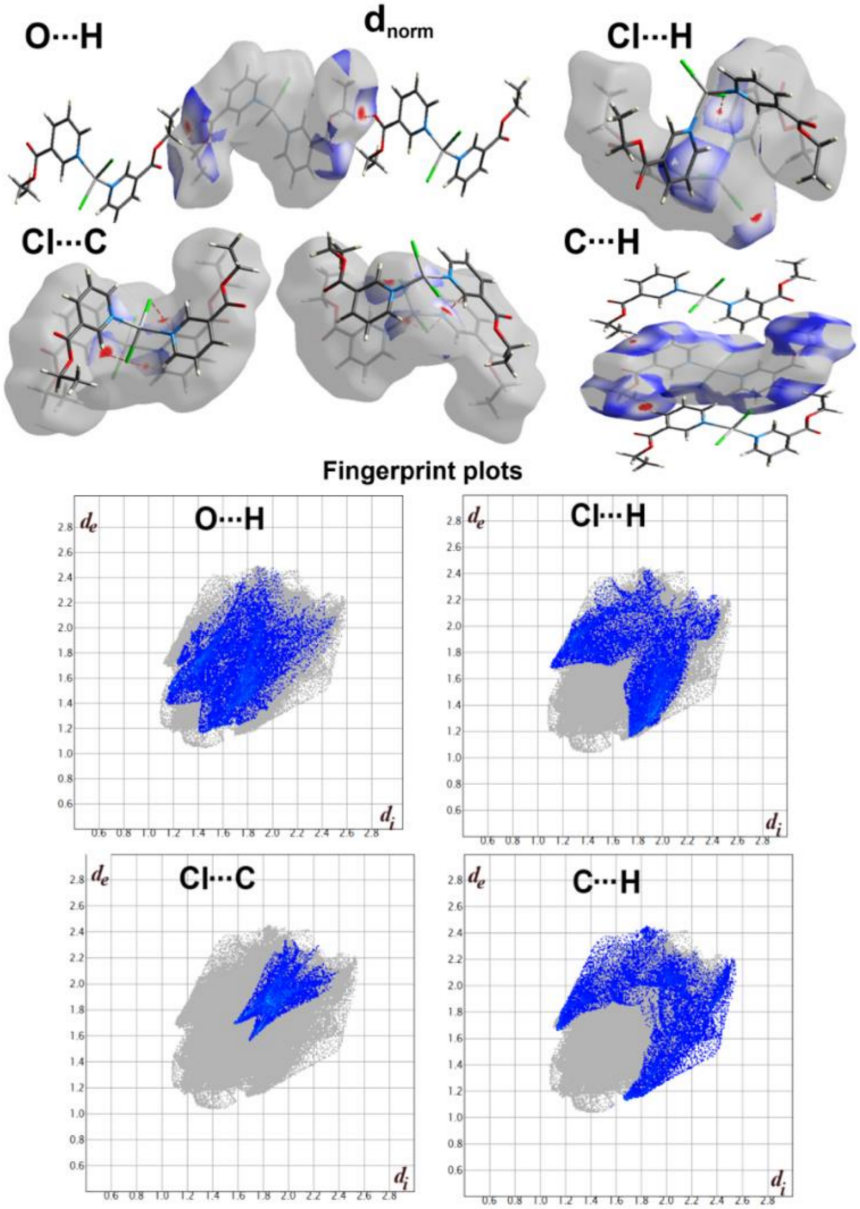

Figure 8. The fingerprint plots (**left**) and d_{norm} maps (**right**) of the short contacts in complex **1**.

Table 7. The distances of all short contacts in **1**.

Contact	Distance (Å)	Contact	Distance(Å)
O4···H31B	2.520	Cl3···C25	3.337
O5···H7A	2.533	Cl4···C29	3.406
Cl4···H29	2.799	Cl4···C17	3.264
Cl1···C9	3.349	C16···H19	2.734
Cl2···C1	3.270	C24···H11	2.604
Cl2···C13	3.396		

For complex **2**, there was disorder in one of the two ethyl groups attached to the amide moiety. As a result, there were two disordered parts, which differed in the orientation of this ethyl group (Figure 4). The fingerprint plot of the two parts was dominated by H···H, O···H, and C···H contacts. The contributions of these contacts to the overall surface were 50.2%, 41.1%, and 7.0%, respectively, for **part 1** and 50.2%, 41.2%, and 7.1% for **part 2**. The other interactions had a negligible effect on the Hirshfeld surface in both forms (Figure S4; Supporting Materials). The d_{norm} maps of the two parts showed that the most important contacts were the polar O···H interactions, which appeared as large intense red spots and sharp spikes in the fingerprint plot, indicating short contacts (Figure 9). The distances of these short contacts are listed in Table 8. The main difference between the results of the two disordered parts is the presence of two extra red spots corresponding to the O10···H31C interaction (2.558 Å) only for **part 2** (Figure 9).

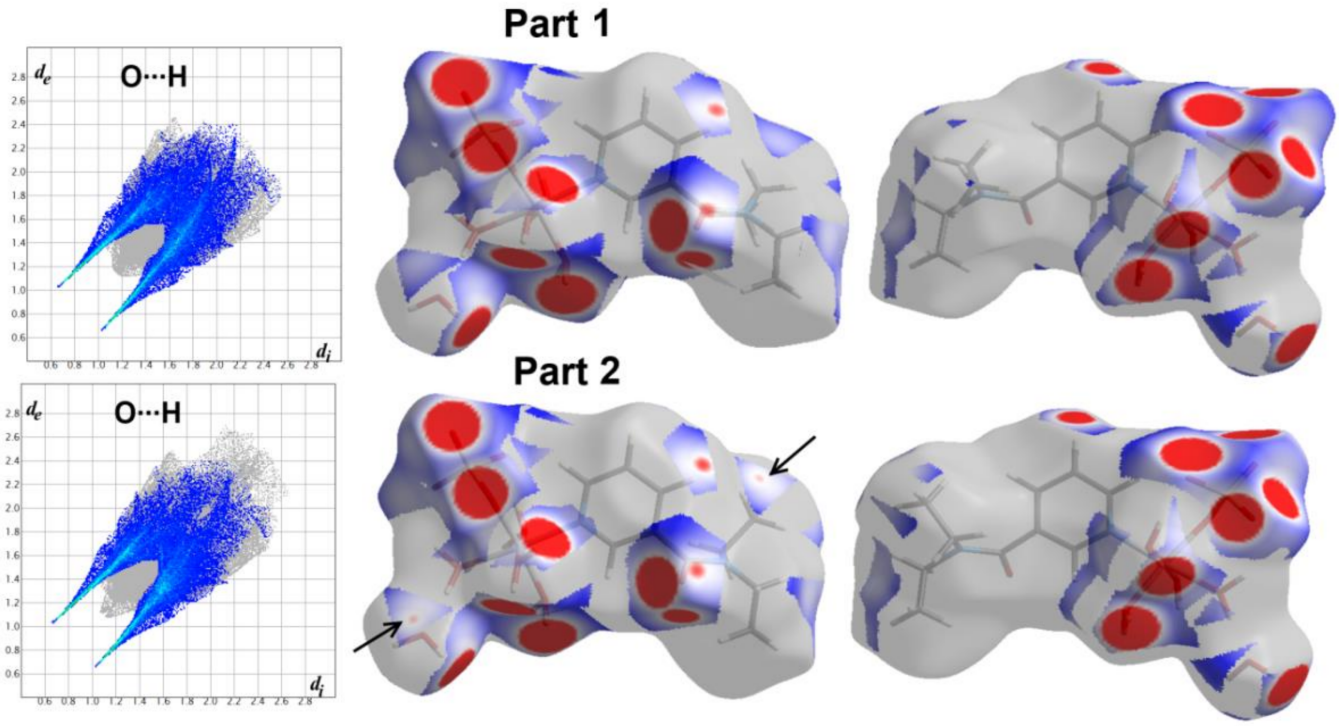

Figure 9. The fingerprint plots and d_{norm} maps related to O···H contacts in **2**. The solid black arrows refer to the extra O10 . . . H31C interactions that exist in **part 2**.

Table 8. The short O···H contacts in complex **2**.

Contact	Distance (Å)	Contact	Distance(Å)
O1 . . . H3	2.502	O7 . . . H4A	1.677
O1 . . . H10A	1.751	O8 . . . H3B	1.851
O1 . . . H2	2.230	O8 . . . H10B	1.918
O6 . . . H3A	1.762	O9 . . . H2A	1.779
O6 . . . H4B	1.754	O10 . . . H31C	2.558

There was another difference between the two disordered parts of complex **2**. In **part 2**, there was one short H···H contact (H14B···H31C) which was not found in **part 1**. The interaction distance of this contact was 2.167 Å. The steep spikes that occurred in the fingerprint plot of **part 2** and the red spot in the corresponding d_{norm} map were additional evidence of the importance of the H···H contacts in **part 2** of complex **2** (Figure 10).

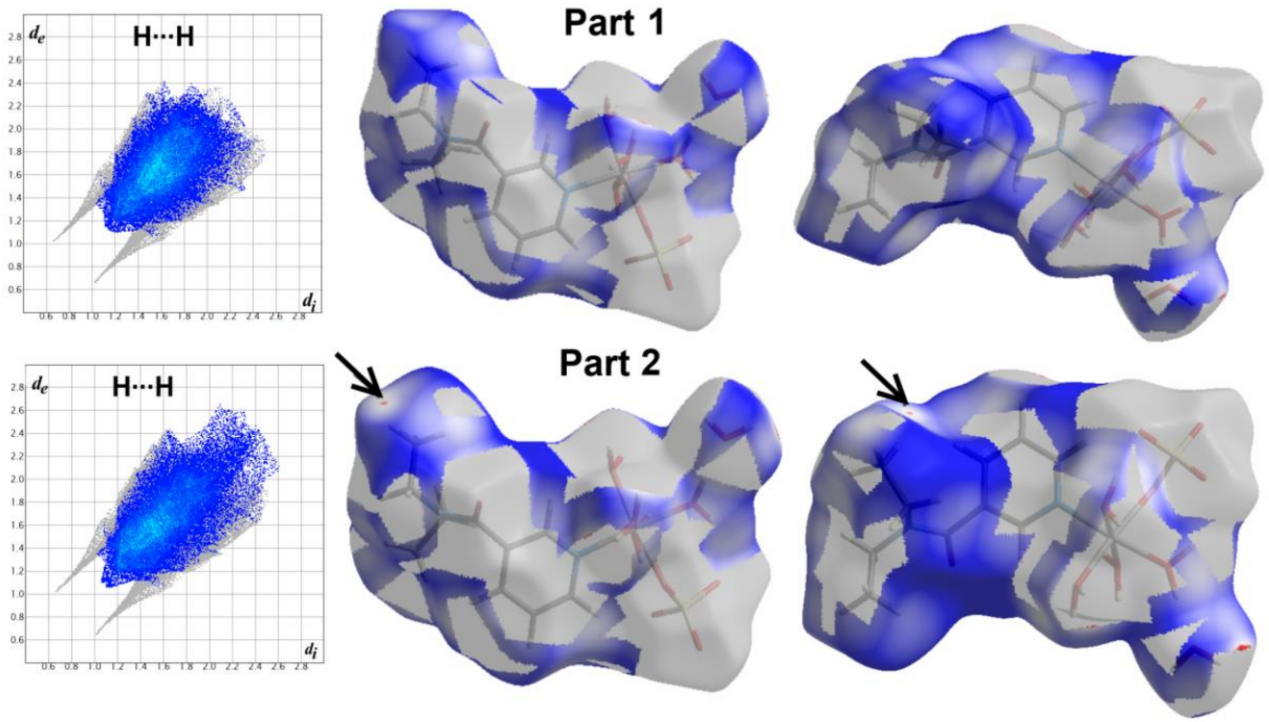

Figure 10. The fingerprint plots and d_{norm} maps related to H···H contacts in **2**. The solid black arrows refer to the extra H14B···H31C interactions that exist in **part 2**.

For complex **3**, the H···H, O···H, and H···C contacts dominated the crystal structure, with 57.1%, 16.9%, and 15.2% contributions, respectively. In addition, there were some minor contributions from N···H, C···C, N···C, and O···C interactions (Figure S5; Supporting Materials). The strong polar O···H interactions appeared as large intense red spots on the d_{norm} map and sharp spikes in the fingerprint plot (Figure 11). The most important O···H interactions occurred between oxygen atoms of the acetate moiety as the hydrogen bond acceptor, with the N-H protons of the amino group as the hydrogen bond donor (Figure 11A). The corresponding O···H contact distances were 1.933 Å (N4-H4E···O1) and 2.005 Å (N3-H3B···O2). Other O···H interactions, such as C7-H7···O3 (2.458 Å), C8-H8···O1 (2.472 Å), C13-H13···O3 (2.473 Å), and C10-H10C···O4 (2.474 Å) occurred with the C-H protons of the picoline moiety as the hydrogen bond donor (Figure 11B).

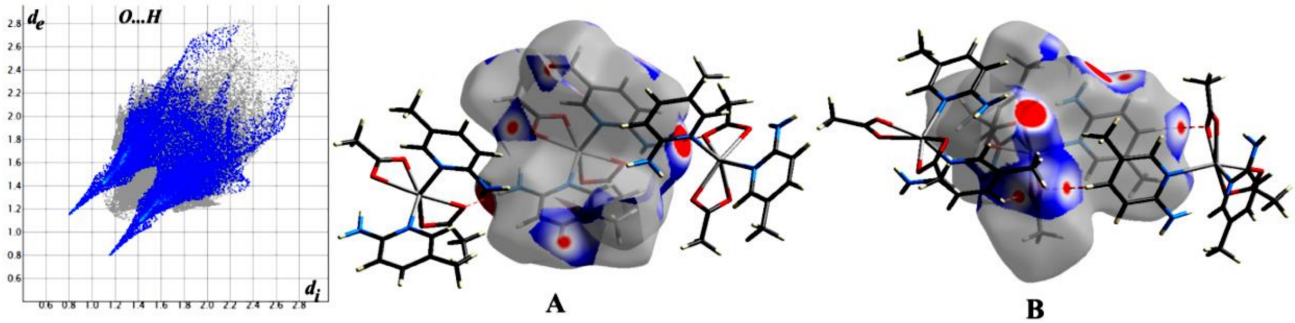

Figure 11. The FP plot and d_{norm} maps showing the different N-H···O (**A**) and C-H···O (**B**) interactions in complex **3**.

In addition, it is important to note the presence of complementary red/blue triangles in the shape index map and the green flat area in the curvedness map. Both indicated the presence of π-π stacking interactions between the nearly parallel stacked pyridine rings (Figure 12). The C5···C7 (3.507 Å) is the shortest distance between the stacked pyridine

rings. This distance was slightly longer than twice that of the vdWs radii (3.40 Å) of the carbon atoms, indicating a relatively weak π-π stacking interaction.

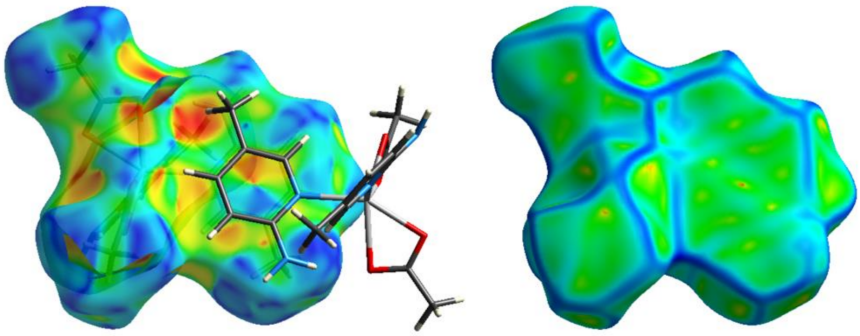

Figure 12. Red/blue triangles in shape index (**left**) and flat green surface in curvedness (**right**) revealed the presence of π-π stacking interaction in **3**.

3.3. Natural Charge Distribution

In metal–organic complexes, the interaction between a metal ion and ligand groups causes considerable changes in their charges as a result of the partial electron density transfer from the ligand (Lewis base) to the metal ion (Lewis acid). The results of their natural charges are listed in Table 9. The calculated natural charges at the central metal ion were 0.8775, 1.0559, and 1.2193 for complexes **1**–**3**, respectively. All values were notably different from the formal charge of +2 for the isolated metal ion. In complex **1**, the Cl^- and **EtNic** ligands transferred 0.406 e and 0.155 e (average values), respectively. In the case of complex **2**, the organic ligand (**DiEtNA**) and the weakly coordinating anion (SO_4^{2-}) transferred lower electron densities of 0.131 and 0.271 e, respectively, to the Zn(II) compared with **1**. In addition, the four coordinated water molecules transferred a net of 0.5421 e to the Zn(II) ion. In complex **3**, the amounts of electrons transferred from each **2Ampic** and OAc^- fragments were 0.1242 and 0.2661 e, respectively. Hence, the net electron densities transferred from the ligand groups to the central metal ion were 1.1226, 0.9441, and 0.78071 e for complexes **1**, **2**, and **3**, respectively. The highest value was found in complex **1**, probably because of the presence of the strongly coordinating Cl^- anion.

Table 9. Charge analysis in complexes **1**, **2**, and **3**.

Moiety	1 (Zn1 Unit)	1 (Zn2 Unit)	Moiety	2	Moiety	3
Zn	0.8775	0.8773	Zn	1.0559	Cd	1.2193
$2Cl^-$	−1.1873	−1.187	SO_4^{2-}	−1.7287	$2OAc^-$	−1.4678 [a]
2(EtNic)	0.3099 [a]	0.3097	DiEtNA	0.1307	2(2Ampic)	0.2484 [a]
			$4H_2O$	0.5421 [a]		

[a] Average value.

3.4. The Atoms in Molecules (AIM) Studies

According to the AIM approach [87–90], each bond has a bond path and a bond critical point [91]. We calculated the AIM parameters of each coordinate bond at its BCP (Table S3 (Supplementary data)). According to the literature, the degree of the electron density function (ρ) at BCP can express the strength of the bond [91]. It is clear that all bonds hadan electron density (ρ) smaller than 0.1 a.u., and the Laplacian ($\nabla^2\rho$) had positive values; this clearly revealed the predominant closed-shell character of the Zn-Cl, Zn-N, Zn-O, Cd-O, and Cd-N bonds, which agrees with their spherical coordination environment, indicating that no specific coordination is preferred and only size determines the number of ligands [92–94]. In addition, large ρ and $\nabla^2\rho$ values indicate that the structure has a high level of local stability [95,96]. As clearly seen in Table S3 (Supplementary data), these parameters were higher for the Zn-N interactions in complex **1** than those in **2**, which agrees

with the shorter Zn-N bonds in the former compared with the latter [97]. Similarly, there are clear inverse correlations between these parameters and Zn-O distances (Figure 13). On the other hand, the quantities of total energy density (H(r)) [98] were near zero, indicating very well that all coordinate bonds have low covalent characters.

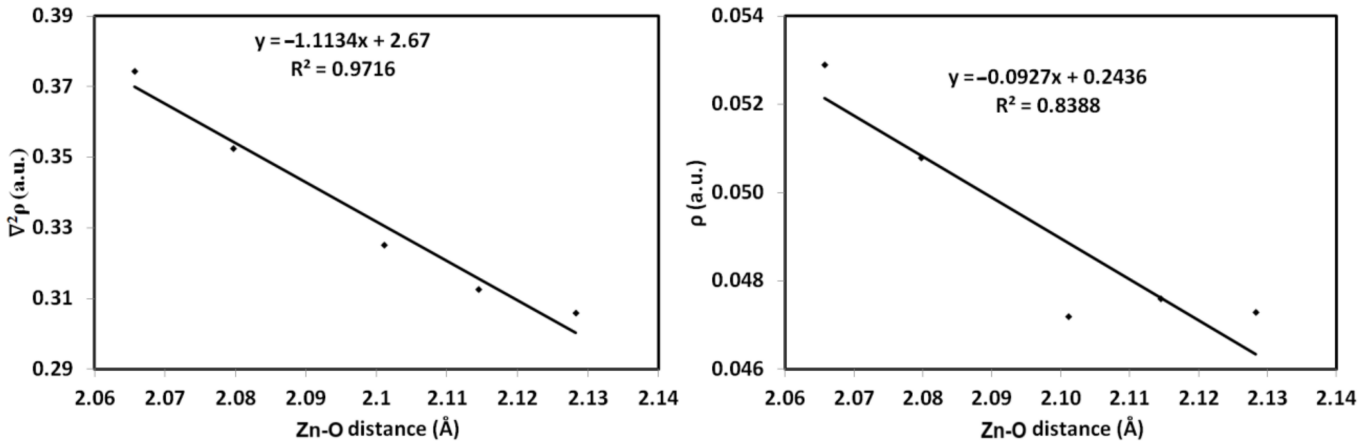

Figure 13. Correlation between the AIM parameters and Zn-O distances.

4. Conclusions

The molecular and supramolecular structures of three heteroleptic complexes of Zn(II) and Cd(II) metal ions with pyridine-type ligands were discussed. The compounds **[Zn(EtNic)$_2$Cl$_2$]**; **1**, **[Zn(DiEtNA)(H$_2$O)$_4$(SO$_4$)]·H$_2$O**; **2**, and **[Cd(OAc)$_2$(2Ampic)$_2$]**; **3** were synthesized by the self-assembly of the corresponding metal(II) salt and the functional pyridine ligand in water–ethanol as solvents. Their single-crystal X-ray structures were determined and analyzed using Hirshfeld analysis. It was found that the Zn(II) was tetra-coordinated in **1** with a distorted tetrahedral coordination environment, while the Zn(II) and Cd(II) were hexa-coordinated in complexes **2** and **3**, respectively. In all complexes, the pyridine ligands were monodentate N-donors via the heterocyclic nitrogen atom. Hirshfeld analysis was used to elucidate the different intermolecular interactions that govern the molecular packing in the studied complexes. DFT calculations of the natural charges predicted decreases in the Zn(II) and Cd(II) natural charges as a consequence of the interactions with the ligand groups. In addition, atoms in molecules (AIM) parameters were used to investigate the nature of the Zn-Cl, Zn-N, Zn-O, Cd-O, and Cd-N coordination interactions. Hence, no specific coordination is preferred, and only size determines the number of ligands around the metal ion.

Supplementary Materials: The following supporting information can be downloaded at: https://www.mdpi.com/article/10.3390/cryst12050590/s1, Table S1: Crystallographic details of complexes **1**–**3**. Table S2: Hydrogen bond parameters (Å, °) in **1**. Table S3: AIM topology parameters (a.u.) at bond critical points (BCPs) as well as the bond distances of the coordinated bonds in complexes **1**, **2**, and **3**. Figure S1: View of the unit cell of **1** along the *ac* plane. Figure S2: View of the unit cell of **2** along the *ac* plane. Figure S3: View of the unit cell of **3** along the *bc* plane. Figure S4: Distribution of all contacts in complexes **1** and **2**. Figure S5: Intermolecular interactions in **3** and their percentages.

Author Contributions: Conceptualization, S.M.S. and M.A.M.A.-Y.; methodology, E.M.F., D.H., J.H.A., A.M.A.B., T.S.K. and A.B.; software, S.M.S., M.S.A., A.M.A.B. and A.B.; formal analysis, E.M.F., D.H., A.M.A.B. and M.S.A.; investigation, S.M.S., A.M.A.B., T.S.K., E.M.F. and D.H.; resources, M.S.A., M.A.M.A.-Y. and A.B.; writing—original draft preparation, S.M.S., E.M.F., M.A.M.A.-Y., A.M.A.B. and A.B.; writing—review and editing, S.M.S., E.M.F., M.A.M.A.-Y., A.M.A.B. and A.B.; supervision, S.M.S. and M.A.M.A.-Y.; project administration, M.S.A., A.B., S.M.S. and M.A.M.A.-Y.; funding acquisition, M.S.A. All authors have read and agreed to the published version of the manuscript.

Funding: Princess Nourah bint Abdulrahman University Researchers Supporting Project number (PNURSP2022R86), Princess Nourah bint Abdulrahman University, Riyadh, Saudi Arabia.

Institutional Review Board Statement: Not applicable.

Informed Consent Statement: Not applicable.

Data Availability Statement: Not applicable.

Acknowledgments: Princess Nourah bint Abdulrahman University Researchers Supporting Project number (PNURSP2022R86), Princess Nourah bint Abdulrahman University, Riyadh, Saudi Arabia.

Conflicts of Interest: The authors declare no conflict of interest.

References

1. Férey, G. Hybrid porous solids: Past, present, future. *Chem. Soc. Rev.* **2008**, *37*, 191–214. [CrossRef]
2. James, S.L. Metal-organic frameworks. *Chem. Soc. Rev.* **2003**, *32*, 276–288. [CrossRef] [PubMed]
3. Chen, B.-L.; Xiang, S.-C.; Qian, G.-D. Metal−Organic Frameworks with Functional Pores for Recognition of Small Molecules. *Acc. Chem. Res.* **2010**, *43*, 1115–1124. [CrossRef] [PubMed]
4. Batten, S.R.; Robson, R. Interpenetrating Nets: Ordered, Periodic Entanglement. *Angew. Chem. Int. Ed.* **1998**, *37*, 1460–1494. [CrossRef]
5. Zaworotko, M.J. Designer pores made easy. *Nature* **2008**, *451*, 410–411. [CrossRef] [PubMed]
6. Neville, S.M.; Halder, G.J.; Chapman, K.W.; Duriska, M.B.; Moubaraki, B.; Murray, K.S.; Kepert, C.J. Guest tunable structure and spin crossover properties in a nanoporous coordination framework material. *J. Am. Chem. Soc.* **2009**, *131*, 12106–12108. [CrossRef] [PubMed]
7. Weng, D.-F.; Wang, Z.-M.; Gao, S. Framework-structured weak ferromagnets. *Chem. Soc. Rev.* **2011**, *40*, 3157–3181. [CrossRef] [PubMed]
8. Li, J.-R.; Sculley, J.; Zhou, H.-C. Metal–Organic Frameworks for Separations. *Chem. Rev.* **2012**, *112*, 869–932. [CrossRef]
9. Maspoch, D.; Ruiz-Molina, D.; Veciana, J. Old materials with new tricks: Multifunctional open-framework materials. *J. Chem. Soc. Rev.* **2007**, *36*, 770–818. [CrossRef]
10. Chen, X.-D.; Du, M.; Mak, T.C.W. Controlled generation of heterochiral or homochiral coordination polymer: Helical conformational polymorphs and argentophilicity-induced spontaneous resolution. *Chem. Commun.* **2005**, *35*, 4417–4419. [CrossRef]
11. Zou, R.-Q.; Sakurai, H.; Xu, Q. Preparation, adsorption properties, and catalytic activity of 3D porous metal-organic frameworks composed of cubic building blocks and alkali-metal ions. *Angew. Chem. Int. Ed.* **2006**, *45*, 2542–2546. [CrossRef]
12. Guo, F.-S.; Leng, J.-D.; Liu, J.-L.; Meng, Z.-S.; Tong, M.-L. Polynuclear and polymeric gadolinium acetate derivatives with large magnetocaloric effect. *Inorg. Chem.* **2012**, *51*, 405–413. [CrossRef]
13. Zhao, H.-Y.; Jin, Z.; Su, H.-M.; Jing, X.-F.; Sun, F.-X.; Zhu, G.-S. Targeted synthesis of a 2D ordered porous organic framework for drug release. *Chem. Commun.* **2011**, *47*, 6389–6391. [CrossRef]
14. Kitagawa, S.; Uemura, K. Dynamic porous properties of coordination polymers inspired by hydrogen bonds. *Chem. Soc. Rev.* **2005**, *34*, 109–119. [CrossRef]
15. Hosseini, M.W. Molecular Tectonics: From Simple Tectons to Complex Molecular Networks. *Acc. Chem. Res.* **2005**, *38*, 313–323. [CrossRef]
16. Du, M.; Zhao, X.-J.; Guo, J.-H.; Batten, S.R. Direction of topological isomers of silver(i) coordination polymers induced by solvent, and selective anion-exchange of a class of PtS-type host frameworks. *Chem. Commun.* **2005**, *38*, 4836–4838. [CrossRef]
17. Zhou, Y.-F.; Hong, M.-C.; Wu, X.-T. Lanthanide–transition metal coordination polymers based on multiple N- and O-donor ligands. *Chem. Commun.* **2006**, *2*, 135–143. [CrossRef]
18. Ockwig, N.W.; Delgado-Friedrichs, O.; O'Keeffe, M.; Yaghi, O.M. Reticular Chemistry: Occurrence and Taxonomy of Nets and Grammar for the Design of Frameworks. *Acc. Chem. Res.* **2005**, *38*, 176–182. [CrossRef]
19. Zhang, W.; Xiong, R.-G.; Huang, S.-D. 3D Framework Containing Cu_4Br_4 Cubane as Connecting Node with Strong Ferroelectricity. *J. Am. Chem. Soc.* **2008**, *130*, 10468–10469. [CrossRef]
20. Zhang, J.-P.; Zhang, Y.-B.; Lin, J.-B.; Chen, X.-M. Metal azolate frameworks: From crystal engineering to functional materials. *Chem. Rev.* **2012**, *112*, 1001–1033. [CrossRef]
21. Zhao, Q.; Li, R.-F.; Xing, S.-K.; Liu, X.-M.; Hu, T.-L.; Bu, X.-H. A Highly Selective On/Off Fluorescence Sensor for Cadmium(II). *Inorg. Chem.* **2011**, *50*, 10041–10046. [CrossRef] [PubMed]
22. Shan, G.-G.; Li, H.-B.; Cao, H.-T.; Zhu, D.-X.; Li, P.; Su, Z.-M.; Liao, Y. Reversible piezochromic behavior of two new cationic iridium(iii) complexes. *Chem. Commun.* **2012**, *48*, 2000–2002. [CrossRef] [PubMed]
23. Li, J.-R.; Kuppler, R.J.; Zhou, H.-C. Selective gas adsorption and separation in metal–organic frameworks. *Chem. Soc. Rev.* **2009**, *38*, 1477–1504. [CrossRef] [PubMed]
24. Hu, Y.-X.; Xiang, S.-C.; Zhang, W.-W.; Zhang, Z.-X.; Wang, L.; Bai, J.-F.; Chen, B.-L. A new MOF-505 analog exhibiting high acetylene storage. *Chem. Commun.* **2009**, *48*, 7551–7553. [CrossRef] [PubMed]
25. Li, X.-Z.; Li, M.-A.; Li, Z.; Hou, J.-Z.; Huang, X.-C.; Li, D. Concomitant and controllable chiral/racemic polymorphs: From achirality to isotactic, syndiotactic, and heterotactic chirality. *Angew. Chem. Int. Ed.* **2008**, *47*, 6371–6374. [CrossRef]
26. Lang, J.; Vagnerova, K.; Czernek, J.; Lhotak, P. Flip–flop Motion of Circular Hydrogen Bond Array in Thiacalix [4]arene. *Supramol. Chem.* **2006**, *18*, 371–381. [CrossRef]

27. Srivastava, K.; Khan, E.; Shimpi, M.R.; Tandon, P.; Sinha, K.; Velaga, S.P. Molecular structure and hydrogen bond interactions of a paracetamol–4,4′-bipyridine cocrystal studied using a vibrational spectroscopic and quantum chemical approach. *CrystEngComm* **2018**, *20*, 213–222. [CrossRef]
28. Perpetuo, G.J.; Janczak, J. Supramolecular architectures in crystals of melamine and aromatic carboxylic acids. *J. Mol. Struct.* **2008**, *891*, 429–436. [CrossRef]
29. Roesky, H.W.; Andruh, M. The interplay of coordinative, hydrogen bonding and π–π stacking interactions in sustaining supramolecular solid-state architectures. A study case of bis(4-pyridyl)- and bis(4-pyridyl-N-oxide) tectons. *Coord. Chem. Rev.* **2003**, *236*, 91–119. [CrossRef]
30. Han, L.L.; Li, Z.H.; Chen, J.S.; Wang, X.P.; Sun, D. Solution and Mechanochemical Syntheses of Two Novel Cocrystals: Ligand Length Modulated Interpenetration of Hydrogen-Bonded 2D 63-hcb Networks Based on a Robust Trimeric Heterosynthon. *Cryst. Growth Des.* **2014**, *14*, 1221–1226. [CrossRef]
31. Sun, D.; Liu, F.J.; Huang, R.B.; Zheng, L.S. Three guest-dependent nitrate–water aggregations encapsulated in silver(i)–bipyridine supramolecular frameworks. *CrystEngComm* **2012**, *14*, 7872–7876. [CrossRef]
32. Sun, D.; Li, Y.H.; Hao, H.J.; Liu, F.J.; Wen, Y.M.; Huang, R.B.; Zheng, L.S. Solvent-Controlled Rare Case of a Triple Helical Molecular Braid Assembled from Proton-Transferred Sebacic Acid. *Cryst. Growth Des.* **2011**, *11*, 3323–3327. [CrossRef]
33. Benabid, W.; Ouari, K.; Bendia, S.; Bourzami, R.; Ali, M.A. Crystal structure, spectroscopic studies, DFT calculations, cyclic voltammetry and biological activity of a copper (II) Schiff base complex. *J. Mol. Struct.* **2020**, *1203*, 127313. [CrossRef]
34. Salvadeo, E.; Dubois, L.; Latour, J.-M. Trinuclear copper complexes as biological mimics: Ligand designs and reactivities. *Coord. Chem. Rev.* **2018**, *374*, 345–375. [CrossRef]
35. Zhao, Q.-Q.; Wu, X.-H.; Ren, N.; Zhang, J.-J.; Geng, L.-N. Construction of two novel lanthanide complexes supported by 2-bromine-5-methoxybenzoate and 2,2′-bipyridine: Syntheses, crystal structures and thermodynamic properties. *J. Chem. Thermodyn.* **2017**, *113*, 124–131. [CrossRef]
36. Basu, O.; Das, S.K. Supramolecular inorganic chemistry leading to functional materials. *J. Chem. Sci.* **2020**, *132*, 46–77. [CrossRef]
37. Li, S.M.; Zheng, X.J.; Yuan, D.Q.; Ablet, A.; Jin, L.P. In Situ Formed White-Light-Emitting Lanthanide–Zinc–Organic Frameworks. *Inorg. Chem.* **2012**, *51*, 1201–1203. [CrossRef]
38. Tanabe, K.K.; Allen, C.A.; Cohen, S.M. Photochemical Activation of a Metal–Organic Framework to Reveal Functionality. *Angew. Chem. Int. Ed.* **2010**, *49*, 9730–9733. [CrossRef]
39. Feng, R.; Jiang, F.L.; Chen, L.; Yan, C.F.; Wu, M.Y.; Hong, M.C. Exceptionally high H_2 storage by a metal–organic polyhedral framework. *Chem. Commun.* **2009**, *9*, 5296–5298. [CrossRef]
40. Wang, H.L.; Qi, D.D.; Xie, Z.; Cao, W.; Wang, K.; Shang, H.; Jiang, J.Z. Synthesis and decarboxylative Wittig reaction of difluoromethylene phosphobetaine. *Chem. Commun.* **2013**, *49*, 889–891. [CrossRef]
41. Rachuri, Y.; Parmar, B.; Bisht, K.K.; Suresh, E. Solvothermal self-assembly of Cd^{2+} coordination polymers with supramolecular networks involving N-donor ligands and aromatic dicarboxylates: Synthesis, crystal structure and photoluminescence studies. *Dalton Trans.* **2017**, *46*, 3623–3630. [CrossRef]
42. Amiri, M.G.; Morsali, A.; Bigdeli, F. A New Metal–Organic ZnII Supramolecular Assembled via Hydrogen Bonds and N···N Interactions as a New Precursor for Preparation Zinc(II) Oxide Nanoparticles, Thermal, Spectroscopic and Structural Studies. *J. Inorg. Organomet. Polym. Mater.* **2011**, *21*, 195–200. [CrossRef]
43. Cooke, N.H.C.; Viavattene, R.L.; Eksteen, R.; Wong, W.S.; Davies, G.; Karger, B.L. Use of metal ions for selective separations in high-performance liquid chromatography. *J. Chromatogr.* **1978**, *149*, 391–415. [CrossRef]
44. Le Page, J.N.; Lindner, W.; Davies, G.; Seitz, D.E.; Karger, B.L. Resolution of the optical isomers of dansyl amino acids by reversed phase liquid chromatography with optically active metal chelate additives. *Anal. Chem.* **1979**, *51*, 433–435. [CrossRef]
45. Lindner, W. HPLC-Enantiomerentrennung an gebundenen chiralen Phasen. *Nat. Schaften* **1980**, *67*, 354–356. [CrossRef]
46. Uddin, N.; Sirajuddin, M.; Uddin, N.; Ullah, H.; Ali, S.; Tariq, M.; Tirmizi, S.A.; Khan, A.R. Synthesis, spectroscopic characterization, biological screenings, DNA binding study and POM analyses of transition metal carboxylates. *Spectrochim. Acta A* **2015**, *140*, 563–574. [CrossRef]
47. Agarwala, B.V.; Hingorani, M.S. Characteristic IR and Electronic Spectral Studies on Novel Mixed Ligand Complexes of Copper(II) with Thiosemicarbazones and Heterocyclic Bases. *Synth. Synth. React. Inorg. Met.-Org. Chem.* **1990**, *20*, 123–132.
48. Hayashi, M.; Matsushima, S.; Noro, A.; Matsushita, Y. Mechanical Property Enhancement of ABA Block Copolymer-Based Elastomers by Incorporating Transient Cross-Links into Soft Middle Block. *Macromolecules* **2015**, *48*, 421–431. [CrossRef]
49. Chen, Y.N.; Zhao, W.; Zhang, J.C. Preparation of 4-vinylpyridine (4VP) resin and its adsorption performance for heavy metal ions. *RSC Adv.* **2017**, *7*, 4226–4236. [CrossRef]
50. McCurdie, M.P.; Belfiore, L.A. Spectroscopic analysis of transition-metal coordination complexes based on poly(4-vinylpyridine) and dichlorotricarbonylruthenium(II). *Polymer* **1999**, *40*, 2889–2902. [CrossRef]
51. Oconnell, E.M.; Yang, C.Z.; Root, T.W.; Cooper, S.L. Spectroscopic studies of pyridine-containing polyurethanes blended with metal acetates. *Macromolecules* **1996**, *29*, 6002–6010. [CrossRef]
52. Noro, A.; Matsushima, S.; He, X.D.; Hayashi, M.; Matsushita, Y. Thermoreversible Supramolecular Polymer Gels via Metal-Ligand Coordination in an Ionic Liquid. *Macromolecules* **2013**, *46*, 8304–8310. [CrossRef]

53. Martinez-Bulit, P.; Garza-Ortiz, A.; Mijangos, E.; Barron-Sosa, L.; Sanchez-Bartez, F.; Gracia-Mora, I.; Flores-Parra, A.; Contreras, R.; Reedijk, J.; Barba-Behrens, N. 2,6-Bis(2,6-diethylphenyliminomethyl)pyridine coordination compounds with cobalt(II), nickel(II), copper(II), and zinc(II): Synthesis, spectroscopic characterization, X-ray study and in vitro cytotoxicity. *J. Inorg. Biochem.* **2015**, *142*, 1–7. [CrossRef] [PubMed]
54. Pierrat, P.; Gros, P.C.; Fort, Y. Solid phase synthesis of pyridine-based derivatives from a 2-chloro-5-bromopyridine scaffold. *J. Comb. Chem.* **2005**, *7*, 879–886. [CrossRef]
55. Schlosser, M.; Mongin, F. Pyridine elaboration through organometallic intermediates: Regiochemical control and completeness. *Chem. Soc. Rev.* **2007**, *36*, 1161–1172. [CrossRef]
56. Asath, R.M.; Premkumar, R.; Mathavan, T.; Benial, A.M.F. Structural, spectroscopic and molecular docking studies on 2-amino-3-chloro-5-trifluoromethyl pyridine: A potential bioactive agent. *Spectrochim. Acta A Mol. Biomol. Spectrosc.* **2017**, *175*, 51–60. [CrossRef]
57. Jose, S.P.; Mohan, S. Vibrational spectra and normal co-ordinate analysis of 2-aminopyridine and 2-amino picoline. *Spectrochim Acta A Mol. Biomol. Spectrosc.* **2006**, *64*, 240–245. [CrossRef]
58. Machura, B.; Nawrot, I.; Michalik, K.B.; Machura, I.; Nawrot, K. Michalik, Novel thiocyanate complexes of cadmium(II)-Synthesis, spectroscopic characterization, X-ray studies and DFT calculations. *Polyhedron* **2011**, *30*, 2619–2626. [CrossRef]
59. Ma, Q.; Zhu, M.L.; Yuan, C.X.; Feng, S.S.; Lu, L.P.; Wang, Q.M. A Molecular Helix: Self-Assembly of Coordination Polymers from d10 Metal Ions and 1,10-Phenanthroline-5,6-dione (pdon) with the Bridges of SCN− and Cl−Anions. *Cryst. Growth Des.* **2010**, *10*, 1706–1714. [CrossRef]
60. Tao, J.; Tong, M.L.; Chen, X.M. Hydrothermal synthesis and crystal structures of three-dimensional coordination frameworks constructed with mixed terephthalate (tp) and 4,4′-bipyridine (4,4′-bipy) ligands: [M(tp)(4,4′-bipy)] (M = CoII, CdII or ZnII). *J. Chem. Soc. Dalton Trans.* **2000**, *20*, 3669–3674. [CrossRef]
61. Lo, S.M.L.; Chui, S.S.Y.; Shek, L.Y.; Lin, Z.Y.; Zhang, X.X.; Wen, G.H.; Williams, I.D. Solvothermal Synthesis of a Stable Coordination Polymer with Copper-I−Copper-II Dimer Units: $[Cu_4\{1,4\text{-}C_6H_4(COO)_2\}_3(4,4'\text{-bipy})_2]_n$. *J. Am. Chem. Soc.* **2000**, *122*, 6293–6294. [CrossRef]
62. Shi, Z.; Feng, S.H.; Sun, Y.; Hua, J. Novel Coordination Polymers with Mixed Ligands and Orientated Enantiomers. *Inorg. Chem.* **2001**, *40*, 5312–5313. [CrossRef]
63. Konar, S.; Mukherjee, P.S.; Ribas, J.; Drew, M.G.B.; Ribas, J.; Chaudhuri, N.R. Syntheses of Two New 1D and 3D Networks of Cu(II) and Co(II) Using Malonate and Urotropine as Bridging Ligands: Crystal Structures and Magnetic Studies. *Inorg. Chem.* **2003**, *42*, 2545–2552. [CrossRef]
64. Bourosh, P.; Bulhac, I.; Covaci, O.; Zubareva, V.; Mitina, T. Iron(II) Bis-α-Benzyldioximate Complexes with 3- and 4-Pyridine Hemiacetals as Axial Ligands: Synthesis, Structure, and Physicochemical Properties. *Russ. J. Coord. Chem.* **2018**, *44*, 507–517. [CrossRef]
65. Rechitskaya, E.D.; Kuratieva, N.V.; Lider, E.V.; Eremina, J.A.; Klyushova, L.S.; Eltsov, I.V.; Kostin, G.A. Tuning of cytotoxic activity by bio-mimetic ligands in ruthenium nitrosyl complexes. *J. Mol. Struct.* **2020**, *1219*, 128565. [CrossRef]
66. Wang, N.; Sun, X.; Wan, D.; Chen, J.; Li, B. Chloridobis(dimethylglyoximatok^2N,N′)(ethyl pyridine-3-carboxylate*k*N) cobalt(III). *Acta Cryst. E* **2012**, *68*, m20.
67. Yildirim, T.; Köse, D.A.; Avci, G.A.; Þahin, O.; Akkurt, F. Novel coordination compounds: Mn(II), Co(II), Ni(II), Cu(II), and Zn(II) cations with acesulfame/N,N-diethylnicotinamide ligands. *J. Coord. Chem.* **2019**, *72*, 3502–3517. [CrossRef]
68. Bigoli, F.; Braibant, A.; Pellinghelli, M.A.; Tiripicchio, A. The Crystal and Molecular Structure of Diaquobis-(N,N-diethylnicotinamide)-diisothiocyanatozinc. *Acta Cryst. B* **1973**, *29*, 2344. [CrossRef]
69. Cherkasova, T.G.; Pervukhina, N.V.; Kuratieva, N.V.; Cherkasova, E.V.; Isakova, I.V.; Mizinkina, Y.A.; Tatarinova, E.S. Mixed-Ligand Cobalt(II) and Nickel(II) Complexes with N,N,-Diethylpyridine-3-carboxamide: Synthesis and Crystal Structure. *Russ. J. Inorg. Chem.* **2020**, *65*, 1160–1165. [CrossRef]
70. Maa, Z.; Sutradhar, M.; Gurbanov, A.V.; Maharramov, A.M.; Aliyeva, R.A.; Aliyeva, F.S.; Bahmanova, F.N.; Mardanova, V.I.; Chyragov, F.M.; Mahmudov, K.T. Co^{II}, Ni^{II} and $UO_2{}^{II}$ complexes with β-diketones and their arylhydrazone derivatives: Synthesis, structure and catalytic activity in Henry reaction. *Polyhedron* **2015**, *101*, 14–22. [CrossRef]
71. Bykov, M.; Emelina, A.; Kiskin, M.; Sidorov, A.; Aleksandrov, G.; Bogomyakov, A.; Dobrokhotova, Z.; Novotortsev, V.; Eremenko, I. Coordination polymer $[Li_2Co_2(Piv)_6(l\text{-}L)_2]_n$ (L = 2-amino-5-methylpyridine) as a new molecular precursor for $LiCoO_2$ cathode material. *Polyhedron* **2009**, *28*, 3628–3634. [CrossRef]
72. LI, G.-S.; ZHANGJ, H.-L. Synthesis, Characterization And Crystal Structure of A Polymeric Silver(I) Complex With Cytotoxic Property. *Chil. Chem. Soc.* **2015**, *60*, 2677–2680. [CrossRef]
73. Pakhmutova, E.V.; Malkov, A.E.; Mikhailova, T.B.; Sidorov, A.A.; Fomina, I.G.; Aleksandrov, G.G.; Novotortsev, V.M.; Ikorskii, V.N.; Eremenkoa, I.L. Formation of bi and tetranuclear cobalt(II) trimethylacetate complexes with 2amino5methylpyridine and 2,6diaminopyridine. *Russ. Chem. Bullet* **2003**, *52*, 2117–2124. [CrossRef]
74. Sheldrick, G.M. *SADABS, Program for Empirical Absorption Correction of Area Detector Data*; ScienceOpen: Burlington, VT, USA, 1996.
75. Sheldrick, G.M. Crystal structure refinement with SHELXL. *Acta Crystallogr. C Struct. Chem.* **2015**, *71*, 3–8. [CrossRef]
76. Spackman, M.A.; Jayatilaka, D. Hirshfeld Surface Analysis. *CrystEngComm* **2009**, *11*, 19–32. [CrossRef]
77. Hirshfeld, F.L. Bonded-Atom Fragments for Describing Molecular Charge Densities. *Theor. Chim. Acta* **1977**, *44*, 129–138. [CrossRef]

78. Bernstein, J.; Davis, R.E.; Shimoni, L.; Chang, N.-L. Patterns in Hydrogen Bonding: Functionality and Graph Set Analysis in Crystals. *Angew. Chemie Int. Ed. Engl.* **1995**, *34*, 1555–1573. [CrossRef]
79. Frisch, M.J.; Trucks, G.W.; Schlegel, H.B.; Scuseria, G.E.; Robb, M.A.; Cheeseman, J.R.; Scalmani, G.; Barone, V.; Mennucci, B.; Petersson, G.A.; et al. *GAUSSIAN 09*; Revision A02; Gaussian Inc.: Wallingford, CT, USA, 2009.
80. Glendening, E.D.; Reed, A.E.; Carpenter, J.E.; Weinhold, F. *NBO, version 3.1*; CI; University of Wisconsin: Madison, WI, USA, 1998.
81. Adamo, C.; Barone, V. Exchange functionals with improved long-range behavior and adiabatic connection methods without adjustable parameters: The mPW and mPW1PW models. *J. Chem. Phys.* **1998**, *108*, 664–675. [CrossRef]
82. Feller, D. The role of databases in support of computational chemistry calculations. *J. Comp. Chem.* **1996**, *17*, 1571–1586. [CrossRef]
83. Schuchardt, K.L.; Didier, B.T.; Elsethagen, T.; Sun, L.; Gurumoorthi, V.; Chase, J.; Li, J.; Windus, T.L. Basis set exchange: A community database for computational sciences. *J. Chem. Inf. Model.* **2007**, *47*, 1045–1052. [CrossRef] [PubMed]
84. Bader, R.F.W. *Atoms in Molecules: A Quantum Theory*; Oxford University Press: Oxford, UK, 1990.
85. Lu, T.; Chen, F. Multiwfn: A multifunctional wavefunction analyzer. *J. Comp. Chem.* **2012**, *33*, 580–592. [CrossRef]
86. McKinnon, J.J.; Spackman, M.A.; Mitchell, A.S. Novel tools for visualizing and exploring intermolecular interactions in molecular crystals. *Acta Cryst. B* **2004**, *60*, 627–668. [CrossRef]
87. Matta, C.F.; Hernandez-Trujillo, J.; Tang, T.-H.; Bader, R.F.W. Hydrogen–Hydrogen Bonding: A Stabilizing Interaction in Molecules and Crystals. *Chem. Eur. J.* **2003**, *9*, 1940–1951. [CrossRef]
88. Grabowski, S.J.; Pfitzner, A.; Zabel, M.; Dubis, A.T.; Palusiak, M. Intramolecular H···H Interactions for the Crystal Structures of [4-((E)-But-1-enyl)-2,6-dimethoxyphenyl]pyridine-3-carboxylate and [4-((E)-Pent-1-enyl)-2,6-dimethoxyphenyl]pyridine-3-carboxylate; DFT Calculations on Modeled Styrene Derivatives. *J. Phys. Chem. B* **2004**, *108*, 1831–1837. [CrossRef]
89. Matta, C.F.; Castillo, N.; Boyd, R.J. Characterization of a Closed-Shell Fluorine−Fluorine Bonding Interaction in Aromatic Compounds on the Basis of the Electron Density. *J. Phys. Chem. A* **2005**, *109*, 3669–3681. [CrossRef]
90. Pendás, A.M.; Francisco, E.; Blanco, M.A.; Gatti, C. Bond Paths as Privileged Exchange Channels. *Chem. Eur. J.* **2007**, *13*, 9362–9371. [CrossRef]
91. Oliveira, B.G.; Pereira, F.S.; de Araujo, R.C.M.C.; Ramos, M.N. The hdyrogen bond strength: New proposals to evaluate the intermolecular interaction using DFT calculations and the AIM theory. *Chem. Phys. Lett.* **2006**, *427*, 181–184.
92. Bader, R.F.W.; Essén, H. The characterization of atomic interactions. *J. Chem. Phys.* **1984**, *80*, 1943–1960. [CrossRef]
93. Bone, R.G.A.; Bader, R.F.W. Identifying and Analyzing Intermolecular Bonding Interactions in van der Waals Molecules. *J. Phys. Chem.* **1996**, *100*, 10892–10911. [CrossRef]
94. Bobrov, M.F.; Popova, G.V.; Tsirelson, V.G. A topological analysis of electron density and chemical bonding in cyclophosphazenes $P_nN_nX_{2n}$ (X = H, F, Cl; N = 2, 3, 4). *Russ. J. Phys. Chem.* **2006**, *80*, 584–590. [CrossRef]
95. Gatti, C. Chemical bonding in crystals: New directions. *Z. Für Krist.-Cryst. Mater.* **2005**, *220*, 399–457. [CrossRef]
96. Gibbs, G.V.; Downs, R.T.; Cox, D.F.; Ross, N.L.; Boisen, M.B.; Rosso, K.M. Shared and Closed-Shell O−O Interactions in Silicates. *J. Phys. Chem. A* **2008**, *112*, 3693–3699. [CrossRef]
97. Love, I. Polar covalent bonds: An AIM analysis of S,O bonds. *J. Phys. Chem. A* **2009**, *113*, 2640–2646. [CrossRef] [PubMed]
98. Cremer, D.; Kraka, E. Chemical Bonds without Bonding Electron Density—Does the Difference Electron-Density Analysis Suffice for a Description of the Chemical Bond? *Angew. Chem. Int. Ed. Engl.* **1984**, *23*, 627–628. [CrossRef]